The Astrophysical Journal, 817:21 (12pp), 2016 January 20 doi:10.3847/0004-637X/817/1/21

SUPERMASSIVE BLACK HOLES AND THEIR HOST SPHEROIDS. II. THE RED AND BLUE SEQUENCE IN THE $M_{\rm BH}$–$M_{*,\rm SPH}$ DIAGRAM

Giulia A. D. Savorgnan[1], Alister W. Graham[1], Alessandro Marconi[2], and Eleonora Sani[3]
[1] Centre for Astrophysics and Supercomputing, Swinburne University of Technology, Hawthorn, Victoria 3122, Australia; gsavorgn@astro.swin.edu.au
[2] Dipartimento di Fisica e Astronomia, Universitá di Firenze, via G. Sansone 1, I-50019 Sesto Fiorentino, Firenze, Italy
[3] European Southern Observatory, Alonso de Cordova, Vitacura 3107, Santiago, Chile
Received 2015 July 17; accepted 2015 November 23; published 2016 January 19

ABSTRACT

In our first paper, we performed a detailed (i.e., bulge, disks, bars, spiral arms, rings, halo, nucleus, etc.) decomposition of 66 galaxies, with directly measured black hole masses, $M_{\rm BH}$, imaged at 3.6 μm with *Spitzer*. Our sample is the largest to date and, for the first time, the decompositions were checked for consistency with the galaxy kinematics. We present correlations between $M_{\rm BH}$ and the host spheroid (and galaxy) luminosity, $L_{\rm sph}$ (and $L_{\rm gal}$), and also stellar mass, $M_{*,\rm sph}$. While most previous studies have used galaxy samples that were overwhelmingly dominated by high-mass, early-type galaxies, our sample includes 17 spiral galaxies, half of which have $M_{\rm BH} < 10^7\,M_\odot$, and allows us to better investigate the poorly studied low-mass end of the $M_{\rm BH}$–$M_{*,\rm sph}$ correlation. The bulges of early-type galaxies follow $M_{\rm BH} \propto M_{*,\rm sph}^{1.04\pm0.10}$ and define a tight *red sequence* with intrinsic scatter $\epsilon_{(M_{\rm BH}|M_{*,\rm sph})} = 0.43 \pm 0.06$ dex and a median $M_{\rm BH}/M_{*,\rm sph}$ ratio of 0.68 ± 0.04%, i.e., a $\pm2\sigma$ range of 0.1%–5%. At the low-mass end, the bulges of late-type galaxies define a much steeper *blue sequence*, with $M_{\rm BH} \propto M_{*,\rm sph}^{2-3}$ and $M_{\rm BH}/M_{*,\rm sph}$ equal to 0.02% at $M_{\rm BH} \approx 10^6\,M_\odot$. We additionally report that (1) our Sérsic galaxy sample follows $M_{\rm BH} \propto M_{*,\rm sph}^{1.48\pm0.20}$, a less steep sequence than previously reported; (2) bulges with Sérsic index $n_{\rm sph} < 2$, argued by some to be pseudo-bulges, are not offset to lower $M_{\rm BH}$ from the correlation defined by the current bulge sample with $n_{\rm sph} > 2$; and (3) $L_{\rm sph}$ and $L_{\rm gal}$ correlate equally well with $M_{\rm BH}$, in terms of intrinsic scatter, only for early-type galaxies—once reasonable numbers of spiral galaxies are included, the correlation with $L_{\rm sph}$ is better than that with $L_{\rm gal}$.

Key words: black hole physics – galaxies: bulges – galaxies: elliptical and lenticular, cD – galaxies: evolution – galaxies: structure

1. INTRODUCTION

A quarter of a century ago, Dressler (1989) foresaw a "rough scaling of black hole mass with the mass of the spheroidal component" of galaxies, as suggested by the sequence of five galaxies (M87, M104, M31, M32, and the Milky Way). Yee (1992) then announced a linear relation between what was effectively black hole mass and galaxy mass for high-luminosity, bulge-dominated, early-type galaxies radiating near the Eddington limit. This "rough scaling" was a premature version of the early correlations between black hole mass, $M_{\rm BH}$, and host spheroid luminosity, $L_{\rm sph}$, and also host spheroid mass, $M_{\rm sph}$ (Kormendy & Richstone 1995; Magorrian et al. 1998; Marconi & Hunt 2003; Häring & Rix 2004). These initial studies were dominated by high-mass, early-type galaxies, for which they too reported a quasi-linear $M_{\rm BH}$–$M_{\rm sph}$ relation. Subsequent studies of the $M_{\rm BH}$–$L_{\rm sph}$ and $M_{\rm BH}$–$M_{\rm sph}$ diagrams (Ferrarese & Ford 2005; Graham 2007; Lauer et al. 2007a; Gültekin et al. 2009; Sani et al. 2011; Beifiori et al. 2012; Erwin & Gadotti 2012; van den Bosch et al. 2012; Vika et al. 2012; Kormendy & Ho 2013; McConnell & Ma 2013) continued to use galaxy samples dominated by high-mass, early-type systems with $M_{\rm BH} \gtrsim 0.5 \times 10^8\,M_\odot$, and they too recovered a near-linear relation. However, the consensus about a linear $M_{\rm BH}$–$M_{\rm sph}$ correlation was not unanimous. Some studies had reported a slope steeper than one, or noticed that the low-mass spheroids were offset to the right of (or below) the relation traced by the high-mass spheroids (Laor 1998, 2001; Wandel 1999; Ryan et al. 2007). Graham (2012), Graham & Scott (2013), and Scott et al. (2013) found two distinct trends in the $M_{\rm BH}$–$L_{\rm sph}$ and $M_{\rm BH}$–$M_{\rm sph}$ diagrams: a linear and a super-quadratic correlation at the high- and low-mass ends, respectively.[4] Recently, Läsker et al. (2014a; 2014b) derived 2.2 μm bulge luminosities for 35 galaxies (among which only four were classified as spiral galaxies), and reported a slope below unity for their $M_{\rm BH}$–$L_{\rm sph}$ relation. They also claimed that the black hole mass correlates equally well with the total galaxy luminosity as it does with the bulge luminosity.

The $M_{\rm BH}$–$L_{\rm sph}$ relation for early-type (elliptical + lenticular) galaxies can be predicted by combining two other correlations that involve the bulge stellar velocity dispersion, σ. One of these is the $M_{\rm BH}$–σ relation (Ferrarese & Merritt 2000; Gebhardt et al. 2000), which can be described with a single power law ($M_{\rm BH} \propto \sigma^{5-6}$) over a wide range in velocity dispersion (70–350 km s^{-1}, e.g., Graham et al. 2011; McConnell et al. 2011; Graham & Scott 2013). The other is the $L_{\rm sph}$–σ relation, which has long been known to be a "double power law," with $L_{\rm sph} \propto \sigma^{5-6}$ at the luminous end[5] (Schechter 1980; Malumuth & Kirshner 1981; Lauer et al. 2007b; von der Linden et al. 2007; Liu et al. 2008) and $L_{\rm sph} \propto \sigma^2$ at intermediate and faint luminosities (Davies et al. 1983; Held et al. 1992; de Rijcke et al. 2005; Matković & Guzmán 2005; Balcells et al. 2007; Chilingarian et al. 2008; Forbes et al. 2008; Cody et al. 2009; Tortora et al. 2009; Kourkchi

[4] Readers interested in an extensive review about the early discovery and successive improvements of these correlations should consult Graham (2016).
[5] Recent work has the $M_{\rm BH}$–σ correlation as steep as $M_{\rm BH} \propto \sigma^{6.5}$ (Savorgnan & Graham 2015) and the high-luminosity end of the $L_{\rm sph}$–σ correlation as steep as $L_{\rm sph} \propto \sigma^8$ (Montero-Dorta et al. 2015).

et al. 2012). The change in slope of the $L_{\rm sph}$–σ relation occurs at $M_B \approx -20.5$ mag, corresponding to $\sigma \approx 200$ km s^{-1}. The $M_{\rm BH}$–$L_{\rm sph}$ relation should, therefore, be better described by a "broken," rather than a single, power law: with $M_{\rm BH} \propto L_{\rm sph}^{2.5}$ at the low-luminosity end, and $M_{\rm BH} \propto L_{\rm sph}^{1}$ at the high-luminosity end. Due to the scatter in the $M_{\rm BH}$–$L_{\rm sph}$ (or $M_{\rm BH}$–$M_{\rm sph}$) diagram, studies that have not sufficiently probed below $M_{\rm BH} \approx 10^7\,M_\odot$ can easily miss the change in slope occuring at $M_{\rm BH} \approx 10^{(8\pm1)}\,M_\odot$, and erroneously recover a single log–linear relation.

When Graham (2012) pointed out this overlooked inconsistency between these linear and bent relations, he identified two different populations of galaxies, namely the core-Sérsic spheroids (Graham et al. 2003; Trujillo et al. 2004) and the Sérsic spheroids[6], and attributed the change in slope (from super-quadratic to linear) to their different formation mechanisms. In this scenario, core-Sérsic spheroids are built in dry merger events where the black hole and the bulge grow at the same pace, increasing their mass in lock steps ($M_{\rm BH} \propto L_{\rm sph}^{1}$), whereas Sérsic spheroids originate from gas-rich processes in which the mass of the black hole increases more rapidly than the mass of its host spheroid ($M_{\rm BH} \propto L_{\rm sph}^{2.5}$).

Graham & Scott (2013, hereafter GS13) and Scott et al. (2013) presented separate power-law linear regressions for the Sérsic and core-Sérsic spheroids in the $M_{\rm BH}$–$L_{\rm sph}$ and $M_{\rm BH}$–$M_{*,\rm sph}$ (spheroid stellar mass) diagrams, probing down to $M_{\rm BH} \approx 10^6\,M_\odot$. To obtain their dust-corrected *bulge* magnitudes, they did not perform bulge/disk decompositions, but converted the *B*-band and $K_{\rm S}$-band observed, total *galaxy* magnitudes into bulge magnitudes using a mean statistical bulge-to-total ratio based on each object's morphological type and disk inclination.[7] These mean statistical bulge-to-total ratios were obtained from the results of two-component (Sérsic-bulge/exponential-disk) decompositions in the literature. Here we investigate in more detail the $M_{\rm BH}$–$L_{\rm sph}$ and $M_{\rm BH}$–$M_{*,\rm sph}$ diagrams using state-of-the-art galaxy decompositions (Savorgnan & Graham 2015, hereafter Paper I) for galaxies with directly measured black hole masses. Our galaxies are large and nearby, which allows us to perform accurate multicomponent decompositions (instead of simple bulge/disk decompositions). Our decompositions were performed on 3.6 μm *Spitzer* satellite imagery, which is an excellent proxy for the stellar mass, superior to the *K*-band (Sheth et al. 2010, and references therein). Nine of our galaxies have $M_{\rm BH} \lesssim 10^7\,M_\odot$, which allows us to better constrain the slope of the correlation at the low-mass end. Furthermore, our galaxy sample includes 17 spiral galaxies, representing a notable improvement over past studies dominated by early-type galaxies. In a forthcoming paper, we will explore the relation between the black hole mass and the bulge dynamical mass, $M_{\rm dyn,sph} \propto R_{\rm e}\sigma^2$, and address the issue of a black hole fundamental plane.

2. DATA

Our galaxy sample (see Table 1) consists of 66 objects for which a dynamical measurement of the black hole mass had been tabulated in the literature (by GS13 or Rusli et al. 2013) at the time that we started this project, and for which we were able to obtain useful spheroid parameters from 3.6 μm *Spitzer* satellite imagery.

Spheroid magnitudes were derived from our state-of-the-art galaxy decompositions, which take into account bulge, disks, spiral arms, bars, rings, halo, extended or unresolved nuclear source, and partially depleted core. Kinematical information (Emsellem et al. 2011; Arnold et al. 2014; Scott et al. 2014) was used to confirm the presence of rotationally supported disk components in most early-type (elliptical + lenticular) galaxies, and to identify their extent (intermediate-scale disks that are fully embedded in the bulge, or large-scale disks that encase the bulge and dominate the light at large radii). It is worth stressing that, contrary to common knowledge, the majority of "elliptical" galaxies contain disks, i.e., they are not single-component spheroidal systems. Paper I presents the data set used here, including details about the data reduction process and the galaxy modeling technique that we developed. It also discusses how we estimated the uncertainties[8] on the bulge magnitudes and presents the individual 66 galaxy decompositions, along with a comparison and discussion of past decompositions.

Bulge luminosities[9] (Table 1) from Paper Iwere converted into stellar masses using a constant 3.6 μm mass-to-light ratio, $\Upsilon_{3.6} = 0.6$ (Meidt et al. 2014). We additionally explored a more sophisticated way to compute mass-to-light ratios, using the color-$\Upsilon_{3.6}$ relation published by Meidt et al. (2014), their Equation (4)), which allows one to estimate $\Upsilon_{3.6}$ of a galaxy from its [3.6]–[4.5] color. Individual [3.6]–[4.5] colors[10] were taken from Peletier et al. (2012, column 8 of their Table 1) when available for our galaxies, or were estimated from the bulge stellar velocity dispersion, σ, using the color-σ relation presented by Peletier et al. (2012, their Figure 6). We found that the range in [3.6]–[4.5] color is small (0.06 mag), and thus the range in $\Upsilon_{3.6}$ is also small (0.04). After checking that using a single $\Upsilon_{3.6} = 0.6$, independent of [3.6]–[4.5] color, does not significantly affect the results of our analysis, we decided to use individual, color-dependent mass-to-light ratios.

For each galaxy, the total luminosity (or galaxy luminosity, $L_{\rm gal}$) is the sum of the luminosities of all its sub-components. Due to the complexity of their modeling, four galaxies (see Table 1, column 7) had their galaxy luminosities

[6] Core-Sérsic spheroids have partially depleted cores relative to their outer Sérsic light profile, whereas Sérsic spheroids have no central deficit of stars.

[7] While this resulted in individual bulge magnitudes not being exactly correct, their large sample size allowed them to obtain a reasonable $M_{\rm BH}$–$L_{\rm sph}$ relation for the ensemble.

[8] By comparing, for each of our galaxies, the measurements of the bulge magnitude obtained by different authors with that obtained by us, we estimated the uncertainties on the bulge magnitudes, in effect taking into account systematic errors. Systematic errors include incorrect sky subtraction, inaccurate masking of contaminating sources, imprecise description of the PSF, erroneous choice of model components (for example, when failing to identify a galaxy subcomponent and thus omitting it in the model, or when describing a galaxy sub-component with an inadequate function), the radial extent of the surface brightness profile and one's sampling of this. Most of these factors are not included in popular two-dimensional (2D) fitting codes which report only the statistical errors associated with their fitted parameters. In fact, when performing multicomponent decomposition of high signal-to-noise images of nearby—therefore, well spatially resolved—galaxies, errors are dominated by systematics rather than Poisson noise. Unlike many papers, we believe that we have not underestimated the uncertainties associated to the bulge best-fit parameters.

[9] Following Sani et al. (2011), absolute luminosities were calculated assuming a 3.6 μm solar absolute magnitude of 3.25 mag. Absolute luminosities were not corrected for cosmological redshift dimming (this correction would be as small as -0.02 mag for galaxies at a distance of 40 Mpc or -0.05 mag for galaxies at a distance of 100 Mpc).

[10] These are integrated [3.6]–[4.5] colors, measured in a circular aperture within each galaxy's effective radius.

Table 1
Galaxy Sample

Galaxy	Type	Core	Distance (Mpc)	M_{BH} (10^8 $M_\odot$)	MAG_{sph} (mag)	MAG_{gal} (mag)	[3.6]–[4.5] (mag)	$M_{*,sph}$ (10^{10} $M_\odot$)
(1)	(2)	(3)	(4)	(5)	(6)	(7)	(8)	(9)
IC 1459	E	yes	28.4	24^{+10}_{-10}	$-26.15^{+0.18}_{-0.11}$	-26.15 ± 0.25	−0.12	27^{+3}_{-4}
IC 2560	Sp (bar)	no?	40.7	$0.044^{+0.044}_{-0.022}$	$-22.27^{+0.66}_{-0.58}$	-24.76 ± 0.25	−0.08	$1.0^{+0.7}_{-0.5}$
IC 4296	E	yes?	40.7	11^{+2}_{-2}	$-26.35^{+0.18}_{-0.11}$	-26.35 ± 0.25	−0.12	31^{+3}_{-5}
M31	Sp (bar)	no	0.7	$1.4^{+0.9}_{-0.3}$	$-22.74^{+0.18}_{-0.11}$	-24.67 ± 0.25	−0.09	$1.5^{+0.2}_{-0.2}$
M49	E	yes	17.1	25^{+3}_{-1}	$-26.54^{+0.18}_{-0.11}$	-26.54 ± 0.25	−0.12	39^{+4}_{-6}
M59	E	no	17.8	$3.9^{+0.4}_{-0.4}$	$-25.18^{+0.18}_{-0.11}$	-25.27 ± 0.25	−0.09	14^{+2}_{-2}
M64	Sp	no?	7.3	$0.016^{+0.004}_{-0.004}$	$-21.54^{+0.18}_{-0.11}$	-24.24 ± 0.25	−0.06	$0.64^{+0.07}_{-0.10}$
M81	Sp (bar)	no	3.8	$0.74^{+0.21}_{-0.11}$	$-23.01^{+0.88}_{-0.66}$	-24.43 ± 0.25	−0.09	$1.9^{+1.6}_{-1.1}$
M84	E	yes	17.9	$9.0^{+0.9}_{-0.8}$	$-26.01^{+0.66}_{-0.58}$	-26.01 ± 0.25	−0.10	28^{+20}_{-13}
M87	E	yes	15.6	$58.0^{+3.5}_{-3.5}$	$-26.00^{+0.66}_{-0.58}$	-26.00 ± 0.25	−0.11	26^{+18}_{-12}
M89	E	yes	14.9	$4.7^{+0.5}_{-0.5}$	$-24.48^{+0.66}_{-0.58}$	-24.74 ± 0.25	−0.11	$6.3^{+4.4}_{-2.9}$
M94	Sp (bar)	no?	4.4	$0.060^{+0.014}_{-0.014}$	$-22.08^{+0.18}_{-0.11}$	$\leqslant -23.36$	−0.07	$1.00^{+0.11}_{-0.15}$
M96	Sp (bar)	no	10.1	$0.073^{+0.015}_{-0.015}$	$-22.15^{+0.18}_{-0.11}$	-24.20 ± 0.25	−0.08	$0.97^{+0.11}_{-0.15}$
M104	S0/Sp	yes	9.5	$6.4^{+0.4}_{-0.4}$	$-23.91^{+0.66}_{-0.58}$	-25.21 ± 0.25	−0.12	$3.4^{+2.4}_{-1.6}$
M105	E	yes	10.3	4^{+1}_{-1}	$-24.29^{+0.66}_{-0.58}$	-24.29 ± 0.25	−0.10	$5.6^{+3.9}_{-2.5}$
M106	Sp (bar)	no	7.2	$0.39^{+0.01}_{-0.01}$	$-21.11^{+0.18}_{-0.11}$	-24.04 ± 0.25	−0.08	$0.37^{+0.04}_{-0.06}$
NGC 0524	S0	yes	23.3	$8.3^{+2.7}_{-1.3}$	$-23.19^{+0.18}_{-0.11}$	-24.92 ± 0.25	−0.09	$2.2^{+0.2}_{-0.3}$
NGC 0821	E	no	23.4	$0.39^{+0.26}_{-0.09}$	$-24.00^{+0.88}_{-0.66}$	-24.26 ± 0.25	−0.09	$4.7^{+4.0}_{-2.6}$
NGC 1023	S0 (bar)	no	11.1	$0.42^{+0.04}_{-0.04}$	$-22.82^{+0.18}_{-0.11}$	-24.20 ± 0.25	−0.10	$1.5^{+0.2}_{-0.2}$
NGC 1300	Sp (bar)	no	20.7	$0.73^{+0.69}_{-0.35}$	$-22.06^{+0.66}_{-0.58}$	-24.16 ± 0.25	−0.10	$0.70^{+0.49}_{-0.32}$
NGC 1316	merger	no	18.6	$1.50^{+0.75}_{-0.80}$	$-24.89^{+0.66}_{-0.58}$	-26.48 ± 0.25	−0.10	$9.5^{+6.7}_{-4.3}$
NGC 1332	E/S0	no	22.3	14^{+2}_{-2}	$-24.89^{+0.88}_{-0.66}$	-24.95 ± 0.25	−0.12	$8.2^{+6.8}_{-4.5}$
NGC 1374	E	no?	19.2	$5.8^{+0.5}_{-0.5}$	$-23.68^{+0.18}_{-0.11}$	-23.70 ± 0.25	−0.09	$3.6^{+0.4}_{-0.5}$
NGC 1399	E	yes	19.4	$4.7^{+0.6}_{-0.6}$	$-26.43^{+0.18}_{-0.11}$	-26.46 ± 0.25	−0.12	33^{+4}_{-5}
NGC 2273	Sp (bar)	no	28.5	$0.083^{+0.004}_{-0.004}$	$-23.00^{+0.66}_{-0.58}$	-24.21 ± 0.25	−0.08	$2.0^{+1.4}_{-0.9}$
NGC 2549	S0 (bar)	no	12.3	$0.14^{+0.02}_{-0.13}$	$-21.25^{+0.18}_{-0.11}$	-22.60 ± 0.25	−0.10	$0.35^{+0.04}_{-0.05}$
NGC 2778	S0 (bar)	no	22.3	$0.15^{+0.09}_{-0.10}$	$-20.80^{+0.66}_{-0.58}$	-22.44 ± 0.25	−0.09	$0.25^{+0.18}_{-0.12}$
NGC 2787	S0 (bar)	no	7.3	$0.40^{+0.04}_{-0.05}$	$-20.11^{+0.66}_{-0.58}$	-22.28 ± 0.25	−0.10	$0.12^{+0.08}_{-0.05}$
NGC 2974	Sp (bar)	no	20.9	$1.7^{+0.2}_{-0.2}$	$-22.95^{+0.66}_{-0.58}$	-24.16 ± 0.25	−0.09	$1.8^{+1.3}_{-0.8}$
NGC 3079	Sp (bar)	no?	20.7	$0.024^{+0.024}_{-0.012}$	$-23.01^{+0.66}_{-0.58}$	$\leqslant -24.45$	−0.07	$2.4^{+1.7}_{-1.1}$
NGC 3091	E	yes	51.2	36^{+1}_{-2}	$-26.28^{+0.18}_{-0.11}$	-26.28 ± 0.25	−0.12	30^{+3}_{-5}
NGC 3115	E/S0	no	9.4	$8.8^{+10.0}_{-2.7}$	$-24.22^{+0.18}_{-0.11}$	-24.40 ± 0.25	−0.11	$4.9^{+0.5}_{-0.7}$
NGC 3227	Sp (bar)	no	20.3	$0.14^{+0.10}_{-0.06}$	$-21.76^{+0.66}_{-0.58}$	-24.26 ± 0.25	−0.08	$0.67^{+0.47}_{-0.31}$
NGC 3245	S0 (bar)	no	20.3	$2.0^{+0.5}_{-0.5}$	$-22.43^{+0.18}_{-0.11}$	-23.88 ± 0.25	−0.10	$1.0^{+0.1}_{-0.2}$
NGC 3377	E	no	10.9	$0.77^{+0.04}_{-0.06}$	$-23.49^{+0.66}_{-0.58}$	-23.57 ± 0.25	−0.06	$4.0^{+2.8}_{-1.8}$
NGC 3384	S0 (bar)	no	11.3	$0.17^{+0.01}_{-0.02}$	$-22.43^{+0.18}_{-0.11}$	-23.74 ± 0.25	−0.08	$1.2^{+0.1}_{-0.2}$
NGC 3393	Sp (bar)	no	55.2	$0.34^{+0.02}_{-0.02}$	$-23.48^{+0.66}_{-0.58}$	-25.29 ± 0.25	−0.10	$2.8^{+1.9}_{-1.3}$
NGC 3414	E	no	24.5	$2.4^{+0.3}_{-0.3}$	$-24.35^{+0.18}_{-0.11}$	-24.42 ± 0.25	−0.09	$6.5^{+0.7}_{-1.0}$
NGC 3489	S0/Sp (bar)	no	11.7	$0.058^{+0.008}_{-0.008}$	$-21.13^{+0.66}_{-0.58}$	-23.07 ± 0.25	−0.06	$0.42^{+0.30}_{-0.19}$
NGC 3585	E	no	19.5	$3.1^{+1.4}_{-0.6}$	$-25.52^{+0.66}_{-0.58}$	-25.55 ± 0.25	−0.10	18^{+12}_{-8}
NGC 3607	E	no	22.2	$1.3^{+0.5}_{-0.5}$	$-25.36^{+0.66}_{-0.58}$	-25.45 ± 0.25	−0.10	15^{+10}_{-7}
NGC 3608	E	yes	22.3	$2.0^{+1.1}_{-0.6}$	$-24.50^{+0.66}_{-0.58}$	-24.50 ± 0.25	−0.08	$7.8^{+5.5}_{-3.6}$
NGC 3842	E	yes	98.4	97^{+30}_{-26}	$-27.00^{+0.18}_{-0.11}$	-27.04 ± 0.25	−0.11	61^{+7}_{-9}
NGC 3998	S0 (bar)	no	13.7	$8.1^{+2.0}_{-1.9}$	$-22.32^{+0.88}_{-0.66}$	-23.53 ± 0.25	−0.12	$0.78^{+0.65}_{-0.43}$
NGC 4026	S0 (bar)	no	13.2	$1.8^{+0.6}_{-0.3}$	$-21.58^{+0.88}_{-0.66}$	-23.16 ± 0.25	−0.09	$0.50^{+0.42}_{-0.28}$
NGC 4151	Sp (bar)	no	20.0	$0.65^{+0.07}_{-0.07}$	$-23.40^{+0.66}_{-0.58}$	-24.44 ± 0.25	−0.09	$2.8^{+2.0}_{-1.3}$
NGC 4261	E	yes	30.8	5^{+1}_{-1}	$-25.72^{+0.66}_{-0.58}$	-25.76 ± 0.25	−0.12	18^{+13}_{-8}
NGC 4291	E	yes	25.5	$3.3^{+0.9}_{-2.5}$	$-24.05^{+0.66}_{-0.58}$	-24.05 ± 0.25	−0.11	$3.9^{+2.8}_{-1.8}$
NGC 4388	Sp (bar)	no?	17.0	$0.075^{+0.002}_{-0.002}$	$-21.26^{+0.88}_{-0.66}$	$\leqslant -23.50$	−0.07	$0.46^{+0.39}_{-0.26}$
NGC 4459	S0	no	15.7	$0.68^{+0.13}_{-0.13}$	$-23.48^{+0.66}_{-0.58}$	-24.01 ± 0.25	−0.09	$2.9^{+2.1}_{-1.3}$
NGC 4473	E	no	15.3	$1.2^{+0.4}_{-0.9}$	$-23.88^{+0.66}_{-0.58}$	-24.11 ± 0.25	−0.10	$3.9^{+2.7}_{-1.8}$
NGC 4564	S0	no	14.6	$0.60^{+0.03}_{-0.09}$	$-22.30^{+0.18}_{-0.11}$	-22.99 ± 0.25	−0.11	$0.82^{+0.09}_{-0.12}$
NGC 4596	S0 (bar)	no	17.0	$0.79^{+0.38}_{-0.33}$	$-22.73^{+0.18}_{-0.11}$	-24.18 ± 0.25	−0.08	$1.6^{+0.2}_{-0.2}$
NGC 4697	E	no	11.4	$1.8^{+0.2}_{-0.1}$	$-24.82^{+0.88}_{-0.66}$	-24.94 ± 0.25	−0.09	10^{+8}_{-6}
NGC 4889	E	yes	103.2	210^{+160}_{-160}	$-27.54^{+0.18}_{-0.11}$	-27.54 ± 0.25	−0.12	91^{+10}_{-14}
NGC 4945	Sp (bar)	no?	3.8	$0.014^{+0.014}_{-0.007}$	$-20.96^{+0.66}_{-0.58}$	$\leqslant -23.79$	−0.06	$0.36^{+0.26}_{-0.17}$

Table 1
(Continued)

Galaxy	Type	Core	Distance (Mpc)	M_{BH} (10^8 $M_\odot$)	MAG_{sph} (mag)	MAG_{gal} (mag)	[3.6]–[4.5] (mag)	$M_{*,sph}$ (10^{10} $M_\odot$)
(1)	(2)	(3)	(4)	(5)	(6)	(7)	(8)	(9)
NGC 5077	E	yes	41.2	$7.4^{+4.7}_{-3.0}$	$-25.45^{+0.18}_{-0.11}$	-25.45 ± 0.25	−0.11	15^{+2}_{-2}
NGC 5128	merger	no?	3.8	$0.45^{+0.17}_{-0.10}$	$-23.89^{+0.88}_{-0.66}$	-24.97 ± 0.25	−0.07	$5.0^{+4.2}_{-2.8}$
NGC 5576	E	no	24.8	$1.6^{+0.3}_{-0.4}$	$-24.44^{+0.18}_{-0.11}$	-24.44 ± 0.25	−0.09	$7.1^{+0.8}_{-1.1}$
NGC 5845	S0	no	25.2	$2.6^{+0.4}_{-1.5}$	$-22.96^{+0.88}_{-0.66}$	-23.10 ± 0.25	−0.12	$1.4^{+1.2}_{-0.8}$
NGC 5846	E	yes	24.2	11^{+1}_{-1}	$-25.81^{+0.66}_{-0.58}$	-25.81 ± 0.25	−0.10	22^{+16}_{-10}
NGC 6251	E	yes?	104.6	5^{+2}_{-2}	$-26.75^{+0.18}_{-0.11}$	-26.75 ± 0.25	−0.12	46^{+5}_{-7}
NGC 7052	E	yes	66.4	$3.7^{+2.6}_{-1.5}$	$-26.32^{+0.18}_{-0.11}$	-26.32 ± 0.25	−0.11	33^{+4}_{-5}
NGC 7619	E	yes	51.5	25^{+8}_{-3}	$-26.35^{+0.66}_{-0.58}$	-26.41 ± 0.25	−0.11	33^{+23}_{-15}
NGC 7768	E	yes	112.8	13^{+5}_{-4}	$-26.90^{+0.66}_{-0.58}$	-26.90 ± 0.25	−0.11	57^{+40}_{-26}
UGC 03789	Sp (bar)	no?	48.4	$0.108^{+0.005}_{-0.005}$	$-22.77^{+0.88}_{-0.66}$	-24.20 ± 0.25	−0.07	$1.9^{+1.6}_{-1.0}$

Note. Column *(1)*: Galaxy name. Column *(2)*: morphological type (E = elliptical, S0 = lenticular, Sp = spiral, merger). The morphological classification of four galaxies is uncertain (E/S0 or S0/Sp). The presence of a bar is indicated. Column *(3)*: presence of a partially depleted core. The question mark is used when the classification has come from the velocity dispersion criteria mentioned in Section 2. Column *(4)*: distance. Column *(5)*: black hole mass. Column *(6)*: absolute 3.6 μm bulge magnitude. Bulge magnitudes come from our state-of-the-art multicomponent galaxy decompositions (Paper I), which include bulges, disks, bars, spiral arms, rings, halos, extended or unresolved nuclear sources, and partially depleted cores, and that—for the first time—were checked to be consistent with the galaxy kinematics. The uncertainties were estimated with a method that takes into account systematic errors, which are typically not considered by popular 2D fitting codes. Column *(7)*: absolute 3.6 μm galaxy magnitude. Four galaxies had their magnitudes overestimated, which are given here as upper limits. Column *(8)*: [3.6]–[4.5] color. Column *(9)*: bulge stellar mass.

underestimated[11], which are given here as lower limits. Following GS13, we assumed a fixed uncertainty (0.25 mag) for the absolute galaxy magnitude MAG_{gal}.

The morphological classification (E = elliptical; E/S0 = elliptical/lenticular; S0 = lenticular; S0/Sp = lenticular/spiral; Sp = spiral; and "merger") follows from the galaxy models presented in Paper I. Throughout this paper, we will refer to early-type galaxies (E+S0) and late-type galaxies (Sp). Two galaxies classified as E/S0 are obviously included in the early-type bin, whereas two galaxies classified as S0/Sp and another two classified as mergers are included in neither the early- nor the late-type bins.

The Sérsic/core-Sérsic classification presented in this work comes from the compilation of Savorgnan & Graham (2015), who identified partially depleted cores according to the same criteria used by GS13. When no high-resolution image analysis was available from the literature, they inferred the presence of a partially depleted core based on the stellar velocity dispersion: a spheroid is classified as core-Sérsic if $\sigma > 270$ km s^{-1}, or as Sérsic if $\sigma < 166$ km s^{-1}. All of the galaxies with velocity dispersions between these two limits had high-resolution images available.

3. ANALYSIS

We performed a linear regression analysis of the M_{BH}–L_{gal} (see Table 2), M_{BH}–L_{sph} (see Table 3), and M_{BH}–$M_{*,sph}$ (see Table 4) data, using the BCES code from Akritas & Bershady (1996). We also repeated the analysis using both the FITEXY routine (Press et al. 1992), as modified by Tremaine et al. (2002), and the Bayesian estimator `linmix_err` (Kelly 2007). All of these three linear regression routines account for the intrinsic scatter, but only the last two allow one to quantify it. We report linear regressions, both symmetrical and non-symmetrical, for Sérsic/core-Sérsic and for early-/late-type galaxies. Symmetrical regressions are meant to be compared with theoretical expectations, whereas non-symmetrical forward ($M_{BH}|X$) regressions—which minimize the scatter in the $\log(M_{BH})$ direction—are best used to predict black hole masses.

4. RESULTS AND DISCUSSION

4.1. Black Hole Mass–Galaxy Luminosity

The M_{BH}–L_{gal} diagram is shown in Figure 1. Four spiral galaxies had their total luminosities underestimated (see Table 1) and thus are not included in the linear regression analysis (see Table 2).

Läsker et al. (2014b) analyzed a sample of 35 galaxies, among which only four were classified as spiral galaxies, and claimed that the M_{BH}–L_{sph} and M_{BH}–L_{gal} relations, which they fit with a single power law, have consistent intrinsic scatter. Here, instead, thanks to our galaxy sample that includes 17 spiral galaxies, we show that the claim made by Läsker et al. (2014b) is valid only for early-type galaxies. That is, when considering only early-type galaxies, we find that the M_{BH}–L_{sph} and M_{BH}–L_{gal} relations have the same level of intrinsic scatter. However, our M_{BH}–L_{sph} relation for all 66 galaxies, irrespective of their morphological type, has an intrinsic scatter $\epsilon_{(Y|X)} = 0.51 \pm 0.06$ dex (forward linear regression) and $\epsilon_{(X|Y)} = 0.60 \pm 0.09$ dex (inverse linear regression), whereas our M_{BH}–L_{gal} relation for 62 (=66–4) galaxies has $\epsilon_{(Y|X)} = 0.63 \pm 0.07$ dex and $\epsilon_{(X|Y)} = 0.91 \pm 0.17$ dex. Because the value of the intrinsic scatter depends on the size of the uncertainties associated with the absolute magnitudes,[12] we tested the robustness of our conclusion by increasing the uncertainties associated with the galaxy absolute magnitudes[13]

[11] These four cases are discussed in Paper I.

[12] The smaller (larger) the uncertainties, the larger (smaller) the intrinsic scatter.

[13] The value of the intrinsic scatter obviously depends also on the size of the uncertainties associated with the black hole masses. However, black hole masses and their uncertainties have been estimated by various authors using different methods, thus we have limited to no control on their values.

Table 2
Linear Regression Analysis of the M_{BH}–L_{gal} Diagram

Subsample (size)	Regression	α	β	$\langle MAG_{gal}\rangle$	ϵ	Δ
	$\log[M_{BH}/M_{\odot}] = \alpha + \beta[(MAG_{gal} - \langle MAG_{gal}\rangle)/mag]$					
All (62)	BCES $(Y\|X)$	8.26 ± 0.08	-0.49 ± 0.06	-24.78	⋯	0.64
	mFITEXY $(Y\|X)$	$8.26^{+0.08}_{-0.08}$	$-0.49^{+0.06}_{-0.07}$	-24.78	$0.61^{+0.07}_{-0.06}$	0.64
	linmix_err $(Y\|X)$	8.26 ± 0.09	-0.49 ± 0.07	-24.78	0.63 ± 0.07	0.64
	BCES $(X\|Y)$	8.26 ± 0.12	-1.01 ± 0.15	-24.78	⋯	0.92
	mFITEXY $(X\|Y)$	$8.26^{+0.11}_{-0.12}$	$-1.03^{+0.13}_{-0.16}$	-24.78	$0.88^{+0.10}_{-0.08}$	0.93
	linmix_err $(X\|Y)$	8.26 ± 0.12	-1.02 ± 0.15	-24.78	0.91 ± 0.17	0.93
	BCES Bisector	8.26 ± 0.09	-0.72 ± 0.07	-24.78	⋯	0.71
	mFITEXY Bisector	$8.26^{+0.10}_{-0.10}$	$-0.73^{+0.09}_{-0.10}$	-24.78	⋯	0.71
	linmix_err Bisector	8.26 ± 0.10	-0.72 ± 0.07	-24.78	⋯	0.71
Early-type (E+S0) (45)	BCES $(Y\|X)$	8.56 ± 0.07	-0.44 ± 0.05	-24.88	⋯	0.45
	mFITEXY $(Y\|X)$	$8.56^{+0.06}_{-0.06}$	$-0.42^{+0.05}_{-0.05}$	-24.88	$0.41^{+0.06}_{-0.05}$	0.45
	linmix_err $(Y\|X)$	8.56 ± 0.07	-0.42 ± 0.06	-24.88	0.43 ± 0.06	0.45
	BCES $(X\|Y)$	8.56 ± 0.08	-0.64 ± 0.05	-24.88	⋯	0.53
	mFITEXY $(X\|Y)$	$8.56^{+0.08}_{-0.08}$	$-0.66^{+0.07}_{-0.08}$	-24.88	$0.51^{+0.07}_{-0.06}$	0.55
	linmix_err $(X\|Y)$	8.56 ± 0.09	-0.65 ± 0.08	-24.88	0.53 ± 0.10	0.54
	BCES Bisector	8.56 ± 0.07	-0.53 ± 0.04	-24.88	⋯	0.47
	mFITEXY Bisector	$8.56^{+0.07}_{-0.07}$	$-0.54^{+0.06}_{-0.06}$	-24.88	⋯	0.47
	linmix_err Bisector	8.56 ± 0.08	-0.53 ± 0.05	-24.88	⋯	0.47

Note. For each subsample, we indicate $\langle MAG_{gal}\rangle$, its average value of galaxy magnitudes. In the last two columns, we report ϵ, the intrinsic scatter, and Δ, the total rms scatter in the $\log(M_{BH})$ direction. Four spiral galaxies had their luminosities underestimated and thus are not included in the linear regression analysis (the sample of all galaxies contains 66–4 = 62 objects). When considering all galaxies, irrespective of their morphological type, the M_{BH}–L_{gal} correlation is weaker than the M_{BH}–L_{sph} correlation, in terms of intrinsic scatter. However, when considering only early-type galaxies, the M_{BH}–L_{gal} and M_{BH}–L_{sph} correlations have consistent intrinsic scatter.

(we originally assumed 0.25 mag). The intrinsic scatter of the M_{BH}–L_{gal} relation only becomes smaller than that of the M_{BH}–L_{sph} relation when assuming an uncertainty larger than 0.7 mag for L_{gal}, which would be significantly larger than the typical value commonly recognized in the literature, and would also oddly exceed the typical uncertainty that we estimated for L_{sph}. Hence, we conclude that our determination of the relative intrinsic scatter is reliable and that M_{BH} correlates equally well with L_{sph} and L_{gal} only for early-type galaxies[14], but not for all (early+late-type) galaxies.

4.2. Black Hole Mass–Spheroid Luminosity

The M_{BH}–L_{sph} diagram is shown in Figure 2, and the linear regression analysis is presented in Table 3. Sérsic and core-Sérsic spheroids have slopes consistent with each other (within their 1σ uncertainties), in disagreement with the findings of GS13. The slope that we obtained for core-Sérsic spheroids ($M_{BH} \propto L_{sph}^{1.18\pm0.20}$) is consistent with the slope reported by GS13 in the K_s-band for the same population ($M_{BH} \propto L_{sph}^{1.10\pm0.20}$). However, the slope that we determined for Sérsic spheroids ($M_{BH} \propto L_{sph}^{1.53\pm0.20}$) is notably shallower than that found by GS13 ($M_{BH} \propto L_{sph}^{2.73\pm0.55}$).

Although the Sérsic/core-Sérsic classification used by GS13 slightly differs[15] from the classification used here, the main cause of the inconsistency is that the bulge-to-total ratios obtained from our galaxy decompositions are different from those assumed by GS13 to convert galaxy luminosities into bulge luminosities. Our bulge-to-total ratios for low-luminosity Sérsic spheroids (3.6 μm $MAG_{sph} \gtrsim -22$ mag) are smaller than those used by GS13. The host galaxies of such bulges are late-type, spiral galaxies, which typically present a complex morphology (bars, double bars, embedded disks, nuclear components, etc.). Our galaxy models account for the extra components, while the average bulge-to-total ratios of GS13 were based on less sophisticated Sérsic-bulge/exponential-disk decompositions which overestimated the bulge luminosity. This results in our bulge magnitudes being on average ∼0.7 mag fainter than in GS13, after accounting for the different wavelength of the data. At the same time, our bulge-to-total ratios for the high-luminosity Sérsic spheroids (3.6 μm $MAG_{sph} \lesssim -24$ mag) are on average larger than those adopted by GS13. In this regime, the host systems are early-type galaxies that feature intermediate-scale disks.[16] Past bulge/disk decompositions failed to correctly identify the extent of such disks and treated them as large-scale disks, thus underestimating the bulge luminosity. The magnitudes that we obtained for such spheroids are on average ∼0.5mag brighter than in GS13. These two effects explain the shallower slope that we obtained for the Sérsic spheroids.

The slope that we obtained for Sérsic spheroids (1.53 ± 0.20) is not consistent with the value of 2.5 expected from $M_{BH} \propto \sigma^5$ and $L_{sph} \propto \sigma^2$. In addition, the Sérsic and core-Sérsic spheroids do not appear to define two distinct M_{BH}–L_{sph} sequences. This leads us to investigate substructure

[14] The majority of our early-type galaxies are elliptical galaxies, some of which have a bulge-to-total ratio close to 1 ($L_{gal} \simeq L_{sph}$). One might wonder whether this constitutes a bias in our analysis. However, we checked that M_{BH} correlates equally well with L_{sph} and L_{gal} not only for early-type (elliptical + lenticular) galaxies, but also for lenticular galaxies only.

[15] The classification has changed for the galaxies NGC 1316, NGC 1332, and NGC 3998.

[16] Intermediate-scale disks are disks of stars fully embedded in the spheroidal component of their galaxy. They are typical of "disky" elliptical galaxies (e.g., NGC 3377), but they can also be found in other types of host galaxies. They can be considered an intermediate class between nuclear disks, with sizes of ∼ 10–100 pc, and large-scale disks, that encase the bulge and dominate the light at large radii.

Table 3
Linear Regression Analysis of the M_{BH}–L_{sph} Diagram

Subsample (size)	Regression	α	β	$\langle MAG_{sph}\rangle$	ϵ	Δ
	$\log[M_{BH}/M_{\odot}] = \alpha + \beta[(MAG_{sph} - \langle MAG_{sph}\rangle)/mag]$					
All (66)	BCES ($Y\|X$)	8.16 ± 0.07	-0.44 ± 0.04	-23.86	⋯	0.56
	mFITEXY ($Y\|X$)	$8.17^{+0.06}_{-0.07}$	$-0.43^{+0.03}_{-0.04}$	-23.86	$0.49^{+0.06}_{-0.05}$	0.56
	linmix_err ($Y\|X$)	8.16 ± 0.07	-0.42 ± 0.04	-23.86	0.51 ± 0.06	0.56
	BCES ($X\|Y$)	8.16 ± 0.08	-0.61 ± 0.05	-23.86	⋯	0.68
	mFITEXY ($X\|Y$)	$8.15^{+0.07}_{-0.08}$	$-0.61^{+0.05}_{-0.05}$	-23.86	$0.58^{+0.07}_{-0.06}$	0.68
	linmix_err ($X\|Y$)	8.16 ± 0.09	-0.60 ± 0.06	-23.86	0.60 ± 0.09	0.67
	BCES Bisector	8.16 ± 0.07	-0.52 ± 0.04	-23.86	⋯	0.60
	mFITEXY Bisector	$8.16^{+0.07}_{-0.07}$	$-0.51^{+0.04}_{-0.04}$	-23.86	⋯	0.60
	linmix_err Bisector	8.16 ± 0.08	-0.51 ± 0.03	-23.86	⋯	0.59
$n > 2$ (43)	BCES ($Y\|X$)	8.58 ± 0.07	-0.42 ± 0.06	-24.77	⋯	0.46
	mFITEXY ($Y\|X$)	$8.57^{+0.07}_{-0.06}$	$-0.41^{+0.04}_{-0.04}$	-24.77	$0.38^{+0.06}_{-0.06}$	0.46
	linmix_err ($Y\|X$)	8.56 ± 0.07	-0.39 ± 0.05	-24.77	0.40 ± 0.06	0.46
	BCES ($X\|Y$)	8.58 ± 0.08	-0.58 ± 0.06	-24.77	⋯	0.56
	mFITEXY ($X\|Y$)	$8.56^{+0.08}_{-0.08}$	$-0.57^{+0.06}_{-0.07}$	-24.77	$0.44^{+0.08}_{-0.11}$	0.55
	linmix_err ($X\|Y$)	8.55 ± 0.09	-0.57 ± 0.08	-24.77	0.49 ± 0.10	0.55
	BCES Bisector	8.58 ± 0.07	-0.50 ± 0.05	-24.77	⋯	0.49
	mFITEXY Bisector	$8.57^{+0.07}_{-0.07}$	$-0.49^{+0.05}_{-0.05}$	-24.77	⋯	0.49
	linmix_err Bisector	8.56 ± 0.08	-0.48 ± 0.05	-24.77	⋯	0.49
Core- Sérsic (22)	BCES ($Y\|X$)	9.06 ± 0.09	-0.32 ± 0.11	-25.73	⋯	0.42
	mFITEXY ($Y\|X$)	$9.06^{+0.08}_{-0.09}$	$-0.26^{+0.08}_{-0.07}$	-25.73	$0.36^{+0.09}_{-0.06}$	0.42
	linmix_err ($Y\|X$)	9.04 ± 0.10	-0.24 ± 0.09	-25.73	0.40 ± 0.08	0.42
	BCES ($X\|Y$)	9.06 ± 0.12	-0.65 ± 0.12	-25.73	⋯	0.61
	mFITEXY ($X\|Y$)	$9.03^{+0.15}_{-0.16}$	$-0.72^{+0.17}_{-0.31}$	-25.73	$0.61^{+0.14}_{-0.09}$	0.68
	linmix_err ($X\|Y$)	9.03 ± 0.17	-0.69 ± 0.27	-25.73	0.68 ± 0.30	0.64
	BCES Bisector	9.06 ± 0.10	-0.47 ± 0.08	-25.73	⋯	0.48
	mFITEXY Bisector	$9.05^{+0.12}_{-0.13}$	$-0.47^{+0.12}_{-0.17}$	-25.73	⋯	0.48
	linmix_err Bisector	9.04 ± 0.14	-0.44 ± 0.12	-25.73	⋯	0.46
Sérsic (44)	BCES ($Y\|X$)	7.71 ± 0.09	-0.41 ± 0.08	-22.92	⋯	0.61
	mFITEXY ($Y\|X$)	$7.72^{+0.08}_{-0.09}$	$-0.41^{+0.07}_{-0.08}$	-22.92	$0.54^{+0.08}_{-0.07}$	0.61
	linmix_err ($Y\|X$)	7.73 ± 0.09	-0.41 ± 0.08	-22.92	0.55 ± 0.08	0.61
	BCES ($X\|Y$)	7.71 ± 0.14	-0.86 ± 0.16	-22.92	⋯	0.93
	mFITEXY ($X\|Y$)	$7.72^{+0.14}_{-0.13}$	$-0.86^{+0.13}_{-0.19}$	-22.92	$0.77^{+0.13}_{-0.10}$	0.93
	linmix_err ($X\|Y$)	7.73 ± 0.14	-0.86 ± 0.17	-22.92	0.79 ± 0.20	0.93
	BCES Bisector	7.71 ± 0.10	-0.61 ± 0.08	-22.92	⋯	0.71
	mFITEXY Bisector	$7.72^{+0.11}_{-0.11}$	$-0.61^{+0.10}_{-0.12}$	-22.92	⋯	0.71
	linmix_err Bisector	7.73 ± 0.12	-0.62 ± 0.09	-22.92	⋯	0.71
Early-type (E+S0) (45)	BCES ($Y\|X$)	8.56 ± 0.07	-0.33 ± 0.04	-24.47	⋯	0.46
	mFITEXY ($Y\|X$)	$8.56^{+0.06}_{-0.06}$	$-0.32^{+0.03}_{-0.04}$	-24.47	$0.40^{+0.06}_{-0.05}$	0.46
	linmix_err ($Y\|X$)	8.55 ± 0.07	-0.32 ± 0.04	-24.47	0.41 ± 0.06	0.46
	BCES ($X\|Y$)	8.56 ± 0.08	-0.48 ± 0.05	-24.47	⋯	0.55
	mFITEXY ($X\|Y$)	$8.54^{+0.08}_{-0.08}$	$-0.49^{+0.05}_{-0.06}$	-24.47	$0.49^{+0.08}_{-0.06}$	0.57
	linmix_err ($X\|Y$)	8.55 ± 0.09	-0.48 ± 0.06	-24.47	0.51 ± 0.10	0.56
	BCES Bisector	$\mathbf{8.56 \pm 0.07}$	$\mathbf{-0.40 \pm 0.04}$	$\mathbf{-24.47}$	⋯	**0.49**
	mFITEXY Bisector	$8.55^{+0.07}_{-0.07}$	$-0.41^{+0.04}_{-0.05}$	-24.47	⋯	0.49
	linmix_err Bisector	8.55 ± 0.08	-0.40 ± 0.04	-24.47	⋯	0.49
Late-type (Sp) (17)	BCES ($Y\|X$)	7.18 ± 0.16	-0.79 ± 0.43	-22.33	–	0.70
	mFITEXY ($Y\|X$)	$7.20^{+0.15}_{-0.15}$	$-0.53^{+0.22}_{-0.24}$	-22.33	$0.55^{+0.15}_{-0.10}$	0.63
	linmix_err ($Y\|X$)	7.24 ± 0.19	-0.46 ± 0.32	-22.33	0.63 ± 0.16	0.62
	BCES ($X\|Y$)	7.18 ± 0.29	-1.71 ± 0.71	-22.33	⋯	1.26
	mFITEXY ($X\|Y$)	$7.38^{+0.54}_{-0.36}$	$-2.02^{+0.71}_{-2.13}$	-22.33	$1.09^{+0.41}_{-0.24}$	1.50
	linmix_err ($X\|Y$)	7.34 ± 0.43	-1.93 ± 1.30	-22.33	1.31 ± 0.97	1.43
	BCES Bisector	$\mathbf{7.18 \pm 0.20}$	$\mathbf{-1.15 \pm 0.27}$	$\mathbf{-22.33}$	⋯	**0.88**
	mFITEXY Bisector	$7.26^{+0.40}_{-0.28}$	$-1.03^{+0.33}_{-0.52}$	-22.33	⋯	0.82
	linmix_err Bisector	7.27 ± 0.33	-0.96 ± 0.37	-22.33	⋯	0.78

Note. For each subsample, we indicate $\langle MAG_{sph}\rangle$, its average value of spheroid magnitudes. In the last two columns, we report ϵ, the intrinsic scatter, and Δ, the total rms scatter in the $\log(M_{BH})$ direction. Both the early- and late-type subsamples do not contain the two galaxies classified as S0/Sp and the two galaxies classified as mergers (45+17 = 66-2-2). The bold values are the linear regression parameters quoted in the text.

Table 4
Linear Regression Analysis of the M_{BH}–$M_{*,sph}$ Diagram

Subsample (size)	Regression	α	β	$\langle MAG_{sph}\rangle$	ϵ	Δ
	$\log[M_{BH}/M_\odot] = \alpha + \beta \log[(M_{*,sph}/\langle M_{*,sph}\rangle)]$					
Core-Sérsic (22)	BCES ($Y\|X$)	9.06 ± 0.09	0.86 ± 0.28	$10^{11.28}$	⋯	0.42
	mFITEXY ($Y\|X$)	$9.06^{+0.08}_{-0.08}$	$0.68^{+0.21}_{-0.20}$	$10^{11.28}$	$0.36^{+0.09}_{-0.06}$	0.42
	`linmix_err` ($Y\|X$)	9.04 ± 0.10	0.64 ± 0.25	$10^{11.28}$	0.40 ± 0.09	0.42
	BCES ($X\|Y$)	9.06 ± 0.12	1.70 ± 0.32	$10^{11.28}$	⋯	0.61
	mFITEXY ($X\|Y$)	$9.03^{+0.15}_{-0.16}$	$1.90^{+0.85}_{-0.46}$	$10^{11.28}$	$0.62^{+0.13}_{-0.10}$	0.68
	`linmix_err` ($X\|Y$)	9.03 ± 0.17	1.80 ± 0.70	$10^{11.28}$	0.67 ± 0.30	0.65
	BCES Bisector	9.06 ± 0.10	1.19 ± 0.23	$10^{11.28}$	⋯	0.47
	mFITEXY Bisector	$9.05^{+0.12}_{-0.13}$	$1.12^{+0.35}_{-0.27}$	$10^{11.28}$	⋯	0.46
	`linmix_err` Bisector	9.04 ± 0.14	1.06 ± 0.26	$10^{11.28}$	⋯	0.45
Sérsic (44)	BCES ($Y\|X$)	7.71 ± 0.09	0.95 ± 0.21	$10^{10.25}$	⋯	0.64
	mFITEXY ($Y\|X$)	$7.72^{+0.10}_{-0.09}$	$0.96^{+0.21}_{-0.21}$	$10^{10.25}$	$0.58^{+0.09}_{-0.07}$	0.64
	`linmix_err` ($Y\|X$)	7.73 ± 0.10	0.98 ± 0.24	$10^{10.25}$	0.59 ± 0.08	0.65
	BCES ($X\|Y$)	7.71 ± 0.16	2.52 ± 0.54	$10^{10.25}$	⋯	1.11
	mFITEXY ($X\|Y$)	$7.72^{+0.16}_{-0.16}$	$2.49^{+0.69}_{-0.45}$	$10^{10.25}$	$0.93^{+0.15}_{-0.13}$	1.10
	`linmix_err` ($X\|Y$)	7.73 ± 0.17	2.48 ± 0.59	$10^{10.25}$	0.95 ± 0.27	1.10
	BCES Bisector	7.71 ± 0.11	1.48 ± 0.20	$10^{10.25}$	⋯	0.74
	mFITEXY Bisector	$7.72^{+0.13}_{-0.13}$	$1.49^{+0.33}_{-0.28}$	$10^{10.25}$	⋯	0.74
	`linmix_err` Bisector	7.73 ± 0.14	1.49 ± 0.24	$10^{10.25}$	⋯	0.74
Early-type (E+S0) (45)	BCES ($Y\|X$)	8.56 ± 0.07	0.85 ± 0.12	$10^{10.81}$	⋯	0.48
	mFITEXY ($Y\|X$)	$8.56^{+0.06}_{-0.07}$	$0.83^{+0.11}_{-0.11}$	$10^{10.81}$	$0.42^{+0.07}_{-0.05}$	0.48
	`linmix_err` ($Y\|X$)	8.55 ± 0.07	0.82 ± 0.12	$10^{10.81}$	0.43 ± 0.06	0.48
	BCES ($X\|Y$)	8.56 ± 0.09	1.27 ± 0.13	$10^{10.81}$	⋯	0.59
	mFITEXY ($X\|Y$)	$8.54^{+0.08}_{-0.09}$	$1.32^{+0.18}_{-0.15}$	$10^{10.81}$	$0.53^{+0.08}_{-0.07}$	0.61
	`linmix_err` ($X\|Y$)	8.55 ± 0.09	1.29 ± 0.17	$10^{10.81}$	0.54 ± 0.11	0.59
	BCES Bisector	$\mathbf{8.56 \pm 0.07}$	$\mathbf{1.04 \pm 0.10}$	$\mathbf{10^{10.81}}$	⋯	**0.51**
	mFITEXY Bisector	$8.55^{+0.07}_{-0.08}$	$1.05^{+0.14}_{-0.12}$	$10^{10.81}$	⋯	0.51
	`linmix_err` Bisector	8.55 ± 0.08	1.03 ± 0.10	$10^{10.81}$	⋯	0.51
Late-type (Sp) (17)	BCES ($Y\|X$)	7.18 ± 0.17	1.95 ± 1.52	$10^{10.05}$	⋯	0.74
	mFITEXY ($Y\|X$)	$7.20^{+0.15}_{-0.16}$	$1.22^{+0.70}_{-0.62}$	$10^{10.05}$	$0.59^{+0.16}_{-0.11}$	0.66
	`linmix_err` ($Y\|X$)	7.23 ± 0.19	0.96 ± 0.96	$10^{10.05}$	0.67 ± 0.16	0.65
	BCES ($X\|Y$)	7.18 ± 0.39	5.89 ± 3.40	$10^{10.05}$	⋯	1.70
	mFITEXY ($X\|Y$)	$7.44^{+1.45}_{-0.52}$	$7.14^{+26.31}_{-3.01}$	$10^{10.05}$	$1.49^{+0.56}_{-0.36}$	2.08
	`linmix_err` ($X\|Y$)	7.42 ± 0.64	6.96 ± 6.73	$10^{10.05}$	1.83 ± 1.86	2.03
	BCES Bisector	$\mathbf{7.18 \pm 0.21}$	$\mathbf{3.00 \pm 1.30}$	$\mathbf{10^{10.05}}$	⋯	**0.94**
	mFITEXY Bisector	$\mathbf{7.24^{+1.04}_{-0.39}}$	$\mathbf{2.28^{+1.67}_{-1.01}}$	$\mathbf{10^{10.05}}$	⋯	**0.79**
	`linmix_err` Bisector	7.26 ± 0.47	1.94 ± 1.24	$10^{10.05}$	⋯	0.74

Note. For each subsample, we indicate $\langle M_{*,sph}\rangle$, its average value of spheroid stellar masses. In the last two columns, we report ϵ, the intrinsic scatter, and Δ, the total rms scatter in the $\log(M_{BH})$ direction. The bold values are the linear regression parameters quoted in the text.

in the M_{BH}–L_{sph} diagram for early- and late-type galaxies. First, we checked that the elliptical and lenticular galaxies, taken separately, have slopes consistent with each other, and thus, taken together, they define a single *early-type sequence* in the M_{BH}–L_{sph} diagram. We then fit the early-type galaxies with a single log–linear regression, and obtained $M_{BH} \propto L_{sph}^{1.00\pm0.10}$. We did not find any convincing evidence for the change in slope required for consistency with the M_{BH}–σ and bent L_{sph}–σ correlations. Because the change in slope should occur at $M_{BH} > 10^{8\pm1}\,M_\odot$, but all of the early-type galaxies in our sample have $M_{BH} \gtrsim 10^7\,M_\odot$, one possible explanation is that we are still not probing enough low black hole masses for this subsample. An additional possibility is that there is no sharp transition going from $L_{sph} \propto \sigma^2$ at low luminosities to $L_{sph} \propto \sigma^5$ at high luminosities. Although the knowledge that many "elliptical" galaxies actually contain embedded stellar disks dates back at least three decades (Capaccioli 1987; Carter 1987; Bender 1990; Rix & White 1990, 1992; Scorza & Bender 1990, 1995; Nieto et al. 1991), it is mainly thanks to large integral-field-spectrograph surveys of early-type galaxies, such as the ATLAS^{3D} Project (Cappellari et al. 2011), that our view has been further advanced and it is now commonly accepted that most "elliptical" galaxies contain disks. Past studies that investigated the L_{sph}–σ diagram might have failed to identify and consequently model the disks in intermediate-luminosity, early-type galaxies, thus overestimating L_{sph} and mistakenly producing a sharp bend in the L_{sph}–σ correlation, rather than a continuously curved relation (with $L_{sph} \propto \sigma^{3-4}$ at intermediate luminosities).

For the bulges of late-type galaxies, we obtained $M_{BH} \propto L_{sph}^{2.88\pm0.68}$. From a cursory inspection of Figure 2, one might be tempted to doubt the statistical significance of this "tentative" *late-type sequence*. However, a visual inspection of the plotted data requires one to take into account the error bars when judging-by-eye the strength of a correlation. Similarly, the Pearson's and Spearman's correlation coefficients are not applicable because they do not take into account the error bars

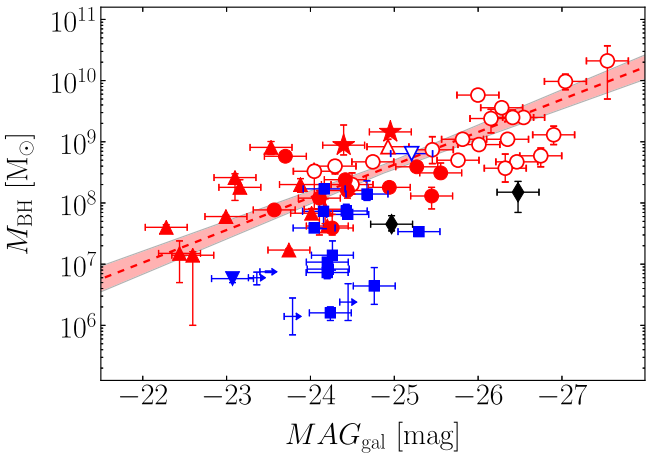

Figure 1. Black hole mass plotted against 3.6 μm galaxy absolute magnitude. Symbols are coded according to the galaxy morphological type: red circle = E, red star = E/S0, red upward triangle = S0, blue downward triangle = S0/Sp, blue square = Sp, black diamond = merger. Empty symbols represent core-Sérsic spheroids, whereas filled symbols are used for Sérsic spheroids. Four spiral galaxies had their magnitudes overestimated (luminosities underestimated) and are shown as upper limits. The red dashed line indicates the BCES bisector linear regression for the 45 early-type galaxies (E+S0), with the red shaded area denoting its 1σ uncertainty. $M_{\rm BH}$ correlates equally well with $L_{\rm gal}$ and $L_{\rm sph}$ only for early-type galaxies, but not for all (early+late-type) galaxies.

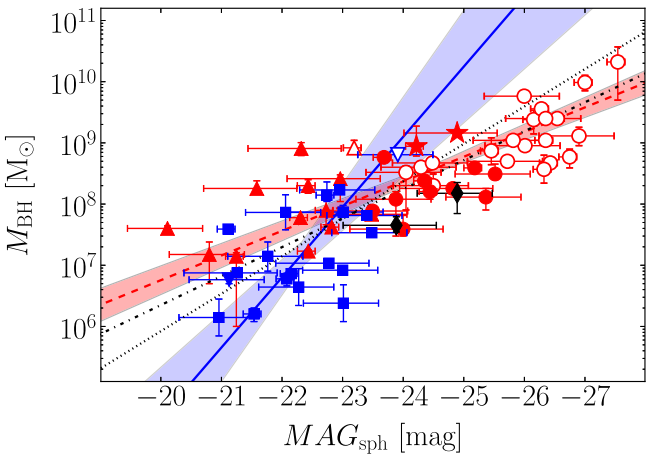

Figure 2. Black hole mass plotted against 3.6 μm spheroid absolute magnitude. Symbols have the same meaning as in Figure 1. The red dashed line indicates the BCES bisector linear regression for the spheroidal component of the 45 early-type (E+S0) galaxies, with the red shaded area denoting its 1σ uncertainty. The blue solid line shows the BCES bisector linear regression for the bulges of the 17 late-type (Sp) galaxies, with the blue shaded area denoting its 1σ uncertainty. The black dashed–dotted and dotted lines represent the BCES bisector linear regressions for the core-Sérsic and Sérsic spheroids, respectively.

on our data. We have, therefore, relied on the quantitative regression analysis.

4.2.1. Pseudo- versus Classical Bulges

Current views distinguish between classical bulges (which are considered to be spheroidal, pressure-supported systems, formed through violent processes, such as hierarchical clustering via minor mergers) and pseudo-bulges (thought to be disk-like, rotation-supported systems, built from secular evolution processes, such as instabilities of their surrounding disk or bar). Pseudo-bulges are notoriously hard to identify

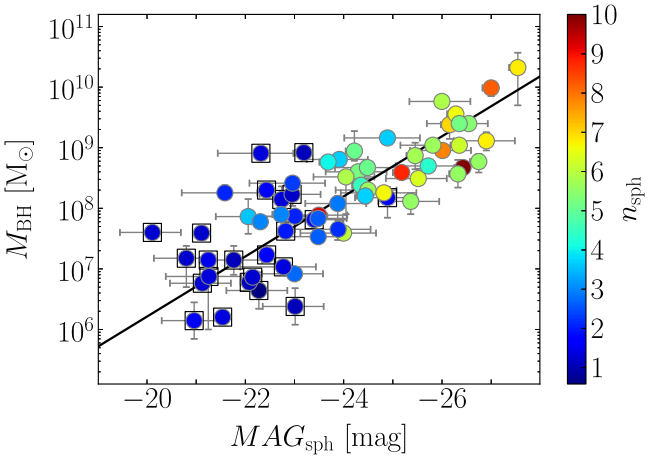

Figure 3. Black hole mass plotted against 3.6 μm spheroid absolute magnitude (as in Figure 2). Symbols are color coded according to the spheroid Sérsic index $n_{\rm sph}$. Bulges with $n_{\rm sph} < 2$, claimed by some to be pseudo-bulges, are enclosed with a square. The black solid line shows the BCES bisector linear regression for the spheroids that have $n_{\rm sph} \geqslant 2$, such that $M_{\rm BH} \propto L_{\rm sph}^{1.25\pm0.13}$.

(Graham 2013, 2014, 2015, 2016). For example, mergers can create bulges that rotate (e.g., Bekki 2010; Keselman & Nusser 2012), and bars can spin-up classical bulges (e.g., Saha et al. 2012; Saha 2015), thus rotation is not a definitive signature of a pseudo-bulge. Furthermore, many galaxies host both a classical and a pseudo-bulge (e.g., Erwin et al. 2003, 2015; Athanassoula 2005; Gadotti 2009; MacArthur et al. 2009; Erwin 2010; dos Anjos & da Silva 2013; Seidel et al. 2015). In the recent literature, pseudo- and classical bulges have frequently been divided at the Sérsic index $n_{\rm sph} = 2$ (e.g., Sani et al. 2011; Beifiori et al. 2012), although, from a selection of hundreds of disk galaxies imaged in the K-band, Graham & Worley (2008) observed no bimodality in the bulge Sérsic indices about $n_{\rm sph} = 2$ or any other value. While pseudo-bulges are expected to have exponential-like surface brightness profiles ($n_{\rm sph} \simeq 1$), being disky components that formed from their surrounding exponential disks (e.g., Bardeen 1975; Hohl 1975; Combes & Sanders 1981; Combes et al. 1990; Pfenniger & Friedli 1991), it has been shown that mergers can create bulges with $n_{\rm sph} < 2$ (e.g., Eliche-Moral et al. 2011; Scannapieco et al. 2011; Querejeta et al. 2015), just as low-luminosity elliptical galaxies (not built from the secular evolution of a disk) are also well known to have $n_{\rm sph} < 2$ and even $n_{\rm sph} < 1$ (e.g., Davies et al. 1988; Young & Currie 1994; Jerjen et al. 2000). The use of the Sérsic index (in addition to rotation) to identify pseudo-bulges is thus a dangerous practice. We therefore do not assume that all bulges with $n_{\rm sph} < 2$ are built from internal processes in the disk (i.e., are what some authors call pseudo-bulges). Sani et al. (2011) reported that pseudo-bulges—which they labelled as such according to the $n_{\rm sph} < 2$ criterion—with low black hole masses ($M_{\rm BH} < 10^7\,M_\odot$) are significantly displaced from the correlation traced by their (classical) bulges with $n_{\rm sph} > 2$. In Figure 3, we show the distribution of spheroid Sérsic indices[17] in the $M_{\rm BH}$–$L_{\rm sph}$ diagram. Our aim is to check whether bulges with $n_{\rm sph} < 2$ are offset to lower black hole masses from the correlation defined by bulges with $n_{\rm sph} > 2$. To do this, we fit a symmetrical linear regression to the bulges that have $n_{\rm sph} > 2$

[17] The spheroid Sérsic indices are taken from our galaxy decompositions (Paper I).

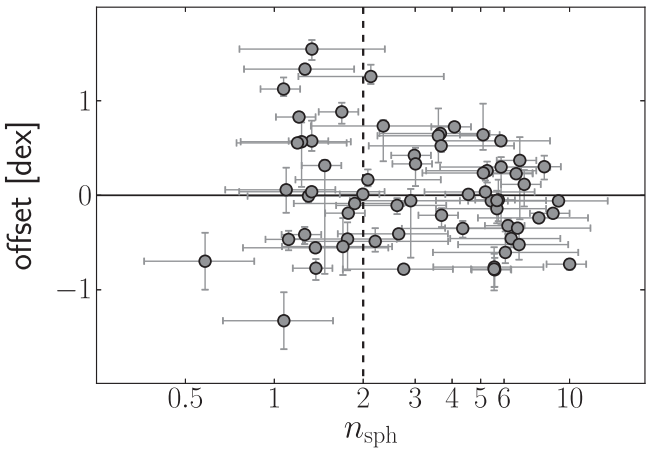

Figure 4. Vertical offset from the $M_{\rm BH}$–$L_{\rm sph}$ correlation defined by spheroids with $n_{\rm sph} \geqslant 2$ (see Figure 3), plotted against $n_{\rm sph}$. The vertical dashed line corresponds to $n_{\rm sph} = 2$. The horizontal solid line is equivalent to a zero vertical offset. Among the bulges with $n_{\rm sph} < 2$, 12 have a positive vertical offset and 11 have a negative vertical offset. Hence, bulges with $n_{\rm sph} < 2$ are not randomly offset to lower black hole masses from the correlation traced by bulges with $n_{\rm sph} \geqslant 2$.

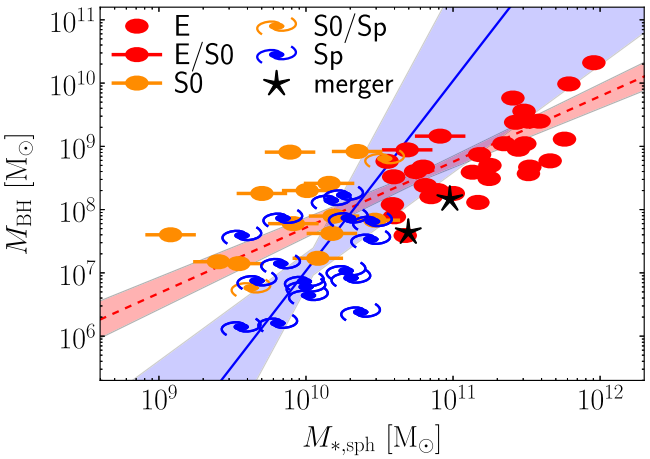

Figure 5. Black hole mass plotted against spheroid stellar mass. Symbols are coded according to the galaxy morphological type (see the legend). The red dashed line indicates the BCES bisector linear regression for the bulges of the 45 early-type galaxies (E+S0), with the red shaded area denoting its 1σ uncertainty. The bulges of early-type galaxies follow $M_{\rm BH} \propto M_{*,\rm sph}^{1.04\pm0.10}$, a near-linear relation consistent with a dry-merging formation scenario. The steeper blue solid line shows the BCES bisector linear regression for the bulges of the 17 late-type (Sp) galaxies, with the blue shaded area denoting its 1σ uncertainty. The bulges of late-type galaxies follow $M_{\rm BH} \propto M_{*,\rm sph}^{2-3}$, indicating that gas-rich processes feed the black hole more efficiently ("quadratically" or "cubically") than the host bulge grows in stellar mass. We note that AGNs with $10^5 \lesssim M_{\rm BH}/M_\odot \lesssim 2 \times 10^6$ (Jiang et al. 2011) appear to follow the blue line (see A. W. Graham et al. 2015, in preparation).

and we then compute the vertical offset of all bulges from this regression. In Figure 4, we plot the vertical offset against $n_{\rm sph}$. Among the 23 bulges with $n_{\rm sph} < 2$, 12 have a positive vertical offset and 11 have a negative vertical offset. Kormendy (2015) provides a list of many pseudo-bulge classification criteria, including the divide at $n_{\rm sph} = 2$, and cautions that each individual criterion has a failure rate of 0%–25%. If this is true, we should find that no less than 75% of bulges with $n_{\rm sph} < 2$ display a negative vertical offset.[18] What we observe, instead, is that there are the same number of bulges with $n_{\rm sph} < 2$ lying above and below the correlation defined by bulges with $n_{\rm sph} > 2$, and that the amplitude of their offset is the same ($\lesssim$1.5 dex). That is, within the current data set, bulges with $n_{\rm sph} < 2$ do not appear to be offset from the correlation traced by bulges with $n_{\rm sph} > 2$.

4.3. Black Hole Mass–Spheroid Stellar Mass

Finally, we present the $M_{\rm BH}$–$M_{*,\rm sph}$ diagram in Figure 5, and its linear regression analysis in Table 4. The bulges of the early-type galaxies follow $M_{\rm BH} \propto M_{*,\rm sph}^{1.04\pm0.10}$, consistent with a dry-merging formation scenario[19], and define a tight *early-type sequence* with intrinsic scatter $\epsilon_{(Y|X)} = 0.43 \pm 0.06$ dex. Graham (2012) reported that the $M_{\rm BH}/M_{\rm dyn,sph}$ ratio for core-Sérsic galaxies was 0.36% ($M_{\rm dyn,sph}$ is the spheroid dynamical mass) and discussed the many implications of this. Using a larger data sample, Graham & Scott (2013) reported that the $M_{\rm BH}/M_{*,\rm sph}$ ratio was 0.49% for core-Sérsic galaxies. Here we find a median $M_{\rm BH}/M_{*,\rm sph}$ ratio of 0.50 ± 0.04% for the 22 core-Sérsic galaxies and 0.68 ± 0.04% for the 45 early-type galaxies. Among other things, this higher value (previously reported to be 0.1%–0.2% for all galaxy types, e.g., Marconi & Hunt 2003), boosts estimates of the black hole mass function and mass density based on galaxy/spheroid luminosity functions.

The bulges of the spiral galaxies trace a steeper *late-type sequence*, whose slope is less well constrained due to the smaller size of the subsample and, more importantly, to the smaller range in $M_{*,\rm sph}$ that the subsample spans. For the bulges of spiral galaxies, the BCES code returns a log–linear relation with a slope $=3.00 \pm 1.30$, while the modified FITEXY routine finds a shallower (but still consistent within the 1σ uncertainty) slope $=2.28^{+1.67}_{-1.01}$. More data would be welcome to better constrain the slope of this *late-type sequence*, though we note that direct measurements of black hole masses below $10^6\,M_\odot$ are extremely challenging to obtain with the current technological resources. In this regard, using a sample of ~140 low-redshift ($z \leqslant 0.35$, with a median redshift $\langle z \rangle = 0.085$) bulges hosting active galactic nuclei (AGNs) with virial black hole masses $10^5 \lesssim M_{\rm BH}/M_\odot \lesssim 2 \times 10^6$ (Jiang et al. 2011), Graham & Scott (2015) showed that they roughly follow the quadratic $M_{\rm BH}$–$M_{*,\rm sph}$ relation defined by their Sérsic bulges. The majority of our spiral galaxies host an AGN[20] and we anticipate here that the correlation traced by our spiral galaxy bulges may track the location of these lower mass AGNs in the $M_{\rm BH}$–$M_{*,\rm sph}$ diagram. That is, the AGNs appear to be the low-mass continuations of our tentative *late-type sequence* shown in Figure 5 and this will be explored with more rigour in a forthcoming paper.

As a final remark, we comment on the work by Reines & Volonteri (2015), who investigated the relationship between black hole mass and total galaxy stellar mass, $M_{*,\rm gal}$. Their

[18] One reaches the same conclusion when using the vertical offset from the correlation defined by bulges with $n_{\rm sph} > 3$ or even $n_{\rm sph} > 4$. There are 13 and 10 bulges with $n_{\rm sph} < 2$ that lie above and below, respectively, the correlation traced by bulges with $n_{\rm sph} > 3$. Similarly, there are 15 and 8 bulges with $n_{\rm sph} < 2$ that lie above and below, respectively, the correlation traced by bulges with $n_{\rm sph} > 4$.

[19] In dry mergers, the black hole and the bulge grow at the same pace, increasing their mass in lock step.

[20] According to the nuclear classification reported on NED (NASA Extragalactic Database), among our 17 spiral galaxies, at least 12 host a Seyfert AGN and one hosts a LINER AGN.

Figure 8 presents the M_{BH}–$M_{*,gal}$ distribution for a sample of ≈260 local AGNs with virial black hole masses and for ≈80 galaxies with dynamical black hole masses. They concluded that the AGN sample and the early-type galaxies with quiescent black holes define two distinct sequences in their M_{BH}–$M_{*,gal}$ diagram; these two sequences have similar slopes, but have normalization factors that are different by more than one order of magnitude. Since we noted that the Jiang et al. (2011) AGN sample follows the steeper M_{BH}–$M_{*,sph}$ correlation traced by our spiral galaxy bulges (the majority of which host an AGN), it would be interesting to recover the M_{BH}–$M_{*,sph}$ distribution also for the AGN sample of Reines & Volonteri (2015). However, we do note that there is emerging evidence (e.g., Busch et al. 2015; Subramanian et al. 2016) for a population of bulges with black hole masses residing below (or to the right of) the red and blue M_{BH}–$M_{*,sph}$ sequences constructed here using samples with directly measured black hole masses, as speculated by Batcheldor (2010).

5. CONCLUSIONS

Using 3.6 μm *Spitzer* images, we have performed accurate multicomponent decompositions (i.e., bulge, disks, bars, spiral arms, rings, halo, nucleus, depleted core, etc.), which were checked to be consistent with the two-dimensional galaxy kinematics, for 66 nearby galaxies with a dynamical measurement of their black hole mass. We have derived galaxy luminosities, spheroid luminosities, and spheroid stellar masses. Our galaxy sample, besides being to date the largest sample with reliable bulge masses used to investigate black hole mass scaling relations, contains 17 spiral galaxies, half of which have $M_{BH} < 10^7\,M_\odot$. This constitutes a significant improvement over past studies whose samples were biased toward high-mass, early-type galaxies.

Using our state-of-the-art data set, we have investigated substructure in the M_{BH}–L_{gal}, M_{BH}–L_{sph} and M_{BH}–$M_{*,sph}$ diagrams. Our principal conclusions are as follows.

1. The logarithmic M_{BH}–$M_{*,sph}$ relation for the spheroidal components of early-type (elliptical + lenticular) galaxies has a slope of 1.04 ± 0.10 and intrinsic scatter of $\epsilon_{(Y|X)} = 0.43 \pm 0.06$ dex. We call this tight correlation an *early-type sequence*. The M_{BH}–$M_{*,sph}$ log-relation for the bulges of late-type (spiral) galaxies has a slope of 2−3, which is less well constrained due to the smaller size of the subsample and, more importantly, the smaller range in spheroid stellar mass ($3 \times 10^9 \lesssim M_{*,sph}/M_\odot \lesssim 3 \times 10^{10}$) that the subsample spans. We refer to this correlation as a *late-type sequence*. In (gas-poor) early-type galaxies, the black hole and the stellar content of the spheroidal component grow at the same pace, following a linear M_{BH}–$M_{*,sph}$ relation. In (gas-rich) spiral galaxies, the black hole grows faster than its host bulge, following a quadratic/cubic M_{BH}–$M_{*,sph}$ relation. Unsurprisingly, in a color–magnitude diagram[21], our early- and late-type galaxies occupy the two distinct regions of the red sequence and the blue cloud, respectively. Analogous with this, we refer to our *early-type sequence* as a *red sequence* and to our *late-type sequence* as a *blue sequence*.
2. The median $M_{BH}/M_{*,sph}$ ratio for the early-type galaxies is $0.68 \pm 0.04\%$. This value is dramatically larger than what was previously reported (0.1%–0.2% for all galaxy types, e.g., Marconi & Hunt 2003), but in close agreement with the value of 0.49% reported by Graham & Scott (2013) for core-Sérsic spheroids.
3. The logarithmic M_{BH}–$M_{*,sph}$ relations for the core-Sérsic and Sérsic spheroids have slopes with overlapping uncertainties (1.19 ± 0.23 and 1.48 ± 0.20, respectively). The Sérsic relation is less steep than, but also has overlapping uncertainties with, the slope of 2.22 ± 0.58 reported by Scott et al. (2013) for Sérsic spheroids. The distinction between core-Sérsic and Sérsic spheroids found by Scott et al. (2013) is thus less pronounced here.
4. In the M_{BH}–L_{sph} (or M_{BH}–$M_{*,sph}$) diagram, for early-type galaxies, we did not observe the change in slope required for consistency with the log–linear M_{BH}–σ and bent L_{sph}–σ correlations. This issue of inconsistency, therefore, remains an open question. It might be that we are still not probing enough low-mass black holes ($M_{BH} < 10^7\,M_\odot$) for the subsample of early-type galaxies, or that the transition from $L_{sph} \propto \sigma^2$ at low luminosities to $L_{sph} \propto \sigma^{(5-6)}$ at high luminosities is less sharp than previously thought. We intend to investigate this point in our future work.
5. It has been argued that pseudo-bulges (disk-like, rotation-supported systems, built from secular processes) do not follow the M_{BH}–L_{sph} correlation defined by classical bulges (spheroidal, pressure-supported systems, formed through violent processes). The recent literature (e.g., Sani et al. 2011; Beifiori et al. 2012) has distinguished between pseudo- and classical bulges according to their Sérsic index, n_{sph}. Although we do not consider the Sérsic index a good indicator of the nature of a bulge (e.g., Graham & Worley 2008), we investigated this point and found that, within the current data set, spheroids with $n_{sph} < 2$ are not offset to lower M_{BH} from the M_{BH}–L_{sph} correlation defined by spheroids with $n_{sph} > 2$.
6. The M_{BH}–L_{gal} and M_{BH}–L_{sph} correlations have the same level of intrinsic scatter when considering early-type galaxies only. Once reasonable numbers of spiral galaxies are included, M_{BH} correlates better with L_{sph} than with L_{gal} (see also Beifiori et al. 2012; Erwin & Gadotti 2012).

Finally, we note that some of the literature-sourced black hole mass measurements used by Kormendy & Ho (2013) are different from those used here. While these differences are smaller than 18% for 78% of the galaxies, in three cases (NGC 0821, NGC 4291, and NGC 3393) they are larger than a factor of 2.3. We repeated our entire analysis using only the 58 galaxies that are in common between our sample and the sample of Kormendy & Ho (2013), assuming for these galaxies the black hole mass measurements published by Kormendy & Ho (2013). In doing so, we found that none of our conclusions changed.

G.S. warmly thanks Luca Cortese, Elisabete Lima Da Cunha, Duncan Forbes, and Gonzalo Diaz for useful discussion. We also thank the anonymous referee for useful comments and suggestions. This research was supported by Australian Research Council funding through grants DP110103509 and FT110100263. This work is based on observations made with the IRAC instrument (Fazio

[21] Total $B - V$ colors, corrected for inclination, Galactic extinction and K-correction, were taken from the HyperLEDA online database (Makarov et al. 2014).

et al. 2004) on board the *Spitzer Space Telescope*, which is operated by the Jet Propulsion Laboratory, California Institute of Technology under a contract with NASA. This research has made use of the GOLDMine database (Gavazzi et al. 2003) and the NASA/IPAC Extragalactic Database (NED) which is operated by the Jet Propulsion Laboratory, California Institute of Technology, under contract with the National Aeronautics and Space Administration. We acknowledge the usage of the HyperLeda database (http://leda.univ-lyon1.fr). The BCES routine (Akritas & Bershady 1996) was run via the python module written by Rodrigo Nemmen (Nemmen et al. 2012), which is available at https://github.com/rsnemmen/BCES.

REFERENCES

Akritas, M. G., & Bershady, M. A. 1996, ApJ, 470, 706
Arnold, J. A., Romanowsky, A. J., Brodie, J. P., et al. 2014, ApJ, 791, 80
Athanassoula, E. 2005, MNRAS, 358, 1477
Balcells, M., Graham, A. W., & Peletier, R. F. 2007, ApJ, 665, 1104
Bardeen, J. M. 1975, in IAU Symp. 69, Dynamics of the Solar Systems, ed. A. Hayli, 297
Batcheldor, D. 2010, ApJL, 711, L108
Beifiori, A., Courteau, S., Corsini, E. M., & Zhu, Y. 2012, MNRAS, 419, 2497
Bekki, K. 2010, MNRAS, 401, L58
Bender, R. 1990, A&A, 229, 441
Busch, G., Fazeli, N., Eckart, A., et al. 2015, arXiv:1511.00904
Capaccioli, M. 1987, IAU Symp. 127, Structure and Dynamics of Elliptical Galaxies, ed. P. T. de Zeeuw, 47
Cappellari, M., Emsellem, E., Krajnović, D., et al. 2011, MNRAS, 413, 813
Carter, D. 1987, ApJ, 312, 514
Chilingarian, I. V., Cayatte, V., Durret, F., et al. 2008, A&A, 486, 85
Cody, A. M., Carter, D., Bridges, T. J., Mobasher, B., & Poggianti, B. M. 2009, MNRAS, 396, 1647
Combes, F., Debbasch, F., Friedli, D., & Pfenniger, D. 1990, A&A, 233, 82
Combes, F., & Sanders, R. H. 1981, A&A, 96, 164
Davies, J. I., Phillipps, S., Cawson, M. G. M., Disney, M. J., & Kibblewhite, E. J. 1988, MNRAS, 232, 239
Davies, R. L., Efstathiou, G., Fall, S. M., Illingworth, G., & Schechter, P. L. 1983, ApJ, 266, 41
de Rijcke, S., Michielsen, D., Dejonghe, H., Zeilinger, W. W., & Hau, G. K. T. 2005, A&A, 438, 491
dos Anjos, S., & da Silva, M. B. 2013, MSAIS, 25, 33
Dressler, A. 1989, in IAU Symp. 134, Active Galactic Nuclei, ed. D. E. Osterbrock & J. S. Miller, 217
Eliche-Moral, M. C., González-García, A. C., Balcells, M., et al. 2011, A&A, 533, A104
Emsellem, E., Cappellari, M., Krajnović, D., et al. 2011, MNRAS, 414, 888
Erwin, P. 2010, arXiv:1002.1445
Erwin, P., Beltrán, J. C. V., Graham, A. W., & Beckman, J. E. 2003, ApJ, 597, 929
Erwin, P., & Gadotti, D. A. 2012, AdAst, 2012, 4
Erwin, P., Saglia, R., Thomas, J., et al. 2015, in IAU Symp. 309, Using 3D Spectroscopy to Probe the Orbital Structure of Composite Bulges, ed. B. L. Ziegler et al., 359
Fazio, G. G., Hora, J. L., Allen, L. E., et al. 2004, ApJS, 154, 10
Ferrarese, L., & Ford, H. 2005, SSRv, 116, 523
Ferrarese, L., & Merritt, D. 2000, ApJL, 539, L9
Forbes, D. A., Lasky, P., Graham, A. W., & Spitler, L. 2008, MNRAS, 389, 1924
Gadotti, D. A. 2009, MNRAS, 393, 1531
Gavazzi, G., Boselli, A., Donati, A., Franzetti, P., & Scodeggio, M. 2003, A&A, 400, 451
Gebhardt, K., Bender, R., Bower, G., et al. 2000, ApJL, 539, L13
Graham, A. 2015, HiA, 16, 360
Graham, A. W. 2007, MNRAS, 379, 711
Graham, A. W. 2012, ApJ, 746, 113
Graham, A. W. 2013, in Elliptical and Disk Galaxy Structure and Modern Scaling, ed. T. D. Oswalt, & W. C. Keel, 91
Graham, A. W. 2014, in ASP Conf. Ser. 480, Structure and Dynamics of Disk Galaxies, ed. M. S. Seigar & P. Treuthardt (San Francisco, CA: ASP), 185
Graham, A. W. 2016, Galactic Bulges, 418, 263
Graham, A. W., Erwin, P., Trujillo, I., & Asensio Ramos, A. 2003, AJ, 125, 2951
Graham, A. W., Onken, C. A., Athanassoula, E., & Combes, F. 2011, MNRAS, 412, 2211
Graham, A. W., & Scott, N. 2013, ApJ, 764, 151
Graham, A. W., & Scott, N. 2015, ApJ, 798, 54
Graham, A. W., & Worley, C. C. 2008, MNRAS, 388, 1708
Gültekin, K., Richstone, D. O., Gebhardt, K., et al. 2009, ApJ, 698, 198
Häring, N., & Rix, H.-W. 2004, ApJL, 604, L89
Held, E. V., de Zeeuw, T., Mould, J., & Picard, A. 1992, in IAU Symp. 149, The Stellar Populations of Galaxies, ed. B. Barbuy & A. Renzini, 429
Hohl, F. 1975, in IAU Symp. 69, Dynamics of the Solar Systems ed. A. Hayli, 349
Jerjen, H., Binggeli, B., & Freeman, K. C. 2000, AJ, 119, 593
Jiang, Y.-F., Greene, J. E., & Ho, L. C. 2011, ApJL, 737, L45
Kelly, B. C. 2007, ApJ, 665, 1489
Keselman, J. A., & Nusser, A. 2012, MNRAS, 424, 1232
Kormendy, J. 2015, arXiv:1504.03330
Kormendy, J., & Ho, L. C. 2013, ARA&A, 51, 511
Kormendy, J., & Richstone, D. 1995, ARA&A, 33, 581
Kourkchi, E., Khosroshahi, H. G., Carter, D., et al. 2012, MNRAS, 420, 2819
Laor, A. 1998, ApJL, 505, L83
Laor, A. 2001, ApJ, 553, 677
Läsker, R., Ferrarese, L., & van de Ven, G. 2014a, ApJ, 780, 69
Läsker, R., Ferrarese, L., van de Ven, G., & Shankar, F. 2014b, ApJ, 780, 70
Lauer, T. R., Faber, S. M., Richstone, D., et al. 2007a, ApJ, 662, 808
Lauer, T. R., Faber, S. M., Richstone, D., et al. 2007b, ApJ, 662, 808
Liu, F. S., Xia, X. Y., Mao, S., Wu, H., & Deng, Z. G. 2008, MNRAS, 385, 23
MacArthur, L. A., González, J. J., & Courteau, S. 2009, MNRAS, 395, 28
Magorrian, J., Tremaine, S., Richstone, D., et al. 1998, AJ, 115, 2285
Makarov, D., Prugniel, P., Terekhova, N., Courtois, H., & Vauglin, I. 2014, A&A, 570, A13
Malumuth, E. M., & Kirshner, R. P. 1981, ApJ, 251, 508
Marconi, A., & Hunt, L. K. 2003, ApJL, 589, L21
Matković, A., & Guzmán, R. 2005, MNRAS, 362, 289
McConnell, N. J., & Ma, C.-P. 2013, ApJ, 764, 184
McConnell, N. J., Ma, C.-P., Gebhardt, K., et al. 2011, Natur, 480, 215
Meidt, S. E., Schinnerer, E., van de Ven, G., et al. 2014, ApJ, 788, 144
Montero-Dorta, A. D., Shu, Y., Bolton, A. S., Brownstein, J. R., & Weiner, B. J. 2015, arXiv:1505.03866
Nemmen, R. S., Georganopoulos, M., Guiriec, S., et al. 2012, Sci, 338, 1445
Nieto, J.-L., Bender, R., Arnaud, J., & Surma, P. 1991, A&A, 244, L25
Peletier, R. F., Kutdemir, E., van der Wolk, G., et al. 2012, MNRAS, 419, 2031
Pfenniger, D., & Friedli, D. 1991, A&A, 252, 75
Press, W. H., Teukolsky, S. A., Vetterling, W. T., & Flannery, B. P. 1992, Numerical Recipes in FORTRAN. The Art of Scientific Computing (2nd ed.; Cambridge: Cambridge Univ. Press)
Querejeta, M., Eliche-Moral, M. C., Tapia, T., et al. 2015, A&A, 573, A78
Reines, A. E., & Volonteri, M. 2015, ApJ, 813, 82
Rix, H.-W., & White, S. D. M. 1990, ApJ, 362, 52
Rix, H.-W., & White, S. D. M. 1992, MNRAS, 254, 389
Rusli, S. P., Thomas, J., Saglia, R. P., et al. 2013, AJ, 146, 45
Ryan, C. J., De Robertis, M. M., Virani, S., Laor, A., & Dawson, P. C. 2007, ApJ, 654, 799
Saha, K. 2015, ApJL, 806, L29
Saha, K., Martinez-Valpuesta, I., & Gerhard, O. 2012, MNRAS, 421, 333
Sani, E., Marconi, A., Hunt, L. K., & Risaliti, G. 2011, MNRAS, 413, 1479
Savorgnan, G. A. D., & Graham, A. W. 2015, MNRAS, 446, 2330
Scannapieco, C., White, S. D. M., Springel, V., & Tissera, P. B. 2011, MNRAS, 417, 154
Schechter, P. L. 1980, AJ, 85, 801
Scorza, C., & Bender, R. 1990, A&A, 235, 49
Scorza, C., & Bender, R. 1995, A&A, 293, 20
Scott, N., Davies, R. L., Houghton, R. C. W., et al. 2014, MNRAS, 441, 274
Scott, N., Graham, A. W., & Schombert, J. 2013, ApJ, 768, 76
Seidel, M. K., Cacho, R., Ruiz-Lara, T., et al. 2015, MNRAS, 446, 2837
Sheth, K., Regan, M., Hinz, J. L., et al. 2010, PASP, 122, 1397
Subramanian, S., Ramya, S., Das, M., et al. 2016, MNRAS, 455, 3148
Tortora, C., Napolitano, N. R., Romanowsky, A. J., Capaccioli, M., & Covone, G. 2009, MNRAS, 396, 1132
Tremaine, S., Gebhardt, K., Bender, R., et al. 2002, ApJ, 574, 740
Trujillo, I., Erwin, P., Asensio Ramos, A., & Graham, A. W. 2004, AJ, 127, 1917
van den Bosch, R. C. E., Gebhardt, K., Gültekin, K., et al. 2012, Natur, 491, 729

Vika, M., Driver, S. P., Cameron, E., Kelvin, L., & Robotham, A. 2012, MNRAS, 419, 2264
von der Linden, A., Best, P. N., Kauffmann, G., & White, S. D. M. 2007, MNRAS, 379, 867
Wandel, A. 1999, ApJL, 519, L39
Yee, H. K. C. 1992, in ASP Conf. Ser. 31, Relationships Between Active Galactic Nuclei and Starburst Galaxies, ed. A. V. Filippenko (San Francisco, CA: ASP), 417
Young, C. K., & Currie, M. J. 1994, MNRAS, 268, L11